Table I. It has a bearing on indications of the existence of semistable states in pion-nucleon scattering[14] and on attempts to use isobaric state models for the theory of the deuteron.[15] The present work was in fact begun under the influence of similar views tentatively considered at this laboratory. The continued lack of success and the possibility of omission of essential elements[14] in the development of fundamental nuclear force theory would make a claim of a connection with the isobaric state of pion-nucleon phenomena rather speculative, especially since there is serious doubt[16] regarding the justification of such an interpretation of the meson data.

ACKNOWLEDGMENTS

The authors would like to express their indebtedness to Mr. A. M. Saperstein for checking many of the transformations, to Miss C. Smolen for computational assistance, and to Mr. R. L. Becker for some check calculations.

---

[14] K. A. Brueckner, Phys. Rev. **86**, 626 (1952). The considerations of Dyson, Bethe, Salpeter, and others, are given in four abstracts from the Cambridge Meeting of the American Physical Society (July, 1953) [Phys. Rev. **90**, 372 (1953)].

[15] H. A. Bethe and N. Austern, Phys. Rev. **86**, 121 (1952); N. Austern, Phys. Rev. **87**, 208 (1952).

[16] Anderson, Fermi, Nagle, and Yodh, Phys. Rev. **86**, 793 (1952); H. L. Anderson and E. Fermi, Phys. Rev. **86**, 794 (1952); Anderson, Fermi, Martin, and Nagle, Phys. Rev. **91**, 155 (1953); E. Fermi and N. Metropolis, Los Alamos unclassified report LA-1492, 1952 (unpublished).

PHYSICAL REVIEW VOLUME 94, NUMBER 3 MAY 1, 1954

Interactions of Negative Pions in Carbon and Lead*

John O. Kessler† and Leon M. Lederman
Columbia University, New York, New York

(Received January 11, 1954)

A cloud chamber investigation of the nuclear interactions of 125-Mev negative pi mesons has been carried out. Carbon and lead were employed as the scattering material. The experimental arrangement was designed to observe the charge-exchange process:

$$\pi^- + \mathrm{C} \rightarrow \mathrm{B}^{(\mathrm{exc})} + [\pi^0 \rightarrow 2\gamma].$$

High-energy photons, probably attributable to charge exchange, are found to arise from nuclear interaction, with a small but finite cross section. Total and differential cross sections for elastic and inelastic scattering, as well as total nuclear reaction cross sections, are presented. A square well (optical model) analysis fits the data with a potential whose real part is attractive and 30 Mev deep, and whose imaginary part corresponds to a mean free path in nuclear matter of 3×10^{-13} cm. The optical model parameters are found to be energy dependent, the well depth increasing and the mean free path decreasing as the energy is raised.

I. INTRODUCTION

A CONSIDERABLE body of experimental fact, relevant to the interaction of pions in complex nuclei, is already established. Nuclear emulsion experiments have demonstrated the principal mechanisms of the interactions,[1] and given information regarding their energy dependence.[2] More recent experiments with counters,[3] cloud chambers,[4] and emulsions,[5] have continued these studies, and have more clearly shown the dependence of these processes on nuclear size.

The following over-all picture presents itself to us: at low energies (0–40 Mev) the dominant process is mesonic absorption with subsequent nuclear excitation resulting in star formation. The star cross section is about half geometric in the 40-Mev region. Only a small elastic scattering cross section is observed. As the bombarding energy increases, both star and elastic cross sections rise. At 60-Mev inelastic scattering begins to occur with an appreciable probability which increases rapidly with energy. The total reaction cross section is nearly geometric at 80 Mev for all complex nuclei. In some cases it seems to rise slowly as higher energies of bombardment are employed.[6]

The picture is completed by consideration of the charge exchange reaction, which is found to be of great

---

* This research was supported by the joint program of the U. S. Office of Naval Research and the U. S. Atomic Energy Commission. A preliminary account of this research was presented at the Cambridge meeting of the American Physical Society, February, 1953 [Phys. Rev. **90**, 342 (1953)].

† Submitted in partial fulfillment of the requirements for the degree of Doctor of Philosophy. Now at RCA Laboratories, Princeton, New Jersey.

[1] Bernardini, Booth, and Lederman, Phys. Rev. **83**, 1277 (1951). This paper may also be used as a summary of references to previous emulsion work; G. Bernardini and F. Levy, Phys. Rev. **84**, 610 (1951); H. Bradner and B. Rankin, Phys. Rev. **87**, 547, 553 (1952).

[2] Bernardini, Booth, and Lederman, Phys. Rev. **83**, 1075 (1951).

[3] Chedester, Isaacs, Sachs, and Steinberger, Phys. Rev. **82**, 958 (1951); R. L. Martin, Phys. Rev. **87**, 1052 (1952); Aarons, Ashkin, Feiner, Gorman, and Smith, Phys. Rev. **90**, 342 (1953); Pevsner, Williams, and Rainwater (private communication).

[4] A. Shapiro, Phys. Rev. **84**, 1063 (1951); Byfield, Kessler, and Lederman, Phys. Rev. **86**, 17 (1952); F. Tenney and J. Tinlot, Phys. Rev. **90**, 342 (1953); Fowler, Fowler, Shutt, Thorndike, and Whittemore, Phys. Rev. **91**, 135 (1953).

[5] S. Goldhaber and G. Goldhaber (private communication); M. Schein, *1953 Rochester Conference* (Interscience Publishers, New York, 1953).

[6] R. L. Martin, Phys. Rev. **87**, 1052 (1952).

importance in high-energy pion-nucleon interactions.[7] The first experiment which sought to find this effect in complex nuclei gave negative results.[8] Relatively low-energy π's (40 Mev) were used. More recently, further experiments concerning this have been performed: in England[9] and Chicago,[10] using nuclear emulsions, at Brookhaven,[11] with cloud chamber techniques, and at Rochester[12] with counters.

The present experiment is one of a series designed to provide data on the elastic, inelastic, and absorption processes of mesons in nuclear matter. It extends the analysis of pion-carbon scattering[13] from 60 to 125 Mev. In addition, information regarding the dependence of these effects on the size of the scattering center is obtained. Lead is employed as the large comparison material. Finally, a search is made for the charge-exchange scattering in these nuclei.

II. EXPERIMENTAL

A. General

A sixteen-inch, rubber diaphragm, expansion cloud chamber, situated in a magnet having a uniform 9000-gauss field, was employed as a detector. In it were placed carbon and lead scattering plates. The disposition of scattering material was determined by the necessity of obtaining optimum observational efficiencies for all processes under simultaneous investigation. The arrangement employed is shown in Fig. 1. A 2.54 cm thick (4.3 g/cm^2) carbon plate is placed across a diameter of the cloud chamber. Parallel with, and one inch away from this plate, on each side, are located two 0.318 cm thick (3.6 g/cm^2$\simeq$0.6 radiation lengths) lead plates. These subtended $\sim$50 percent of the total solid angle at a point in the middle of the carbon plate, on the axis of the cloud chamber. The 135-Mev π^- beam of the Nevis cyclotron was incident upon this arrangement at an angle of $\sim$15° with the normal. Complete attenuation of scatterings near 90° is thereby prevented.

Both the carbon and lead plates were used to gather information concerning scattering and absorption, and to act as conversion material for γ rays produced anywhere in the cloud chamber. The lead plates, in addition, yielded an estimate of the electron contamination of the meson beam. The thickness of the lead plates was chosen as a compromise between the requirements of good conversion efficiency for π^0 gamma rays and small multiple scattering of the resulting electrons. With regard to high-energy elastic scattering, thick scattering plates mean a reduction of the observation efficiency for wide angle events. A correction for this effect may easily be made. For inelastic scattering, where range effects become important, thick scattering plates imply distortion of the differential energy spectrum in addition to reduction in the statistics. It is, however, again generally possible to calculate the correct energy for inelastically scattered tracks, providing they emerge from the plate.

B. Cloud Chamber Operation

The gas filling mixture used was 50 percent argon, 50 percent helium, saturated with 70 percent alcohol $-$30 percent water vapor. The expansion ratio was 1.08. Sweeping fields of from 400 to 900 volts were used. The two lead plates were at high potential, the carbon plate and two conducting coatings on the side wall of the cloud chamber, approximately parallel with the lead plates, were grounded.

The operating cycle of the chamber was of one-minute duration. "Cleaning" operation was secured by two slow expansions, and by an overcompression[14] immediately following the first expansion. The overcompression was made by connecting a small ballast tank under high pressure to the below-diaphragm volume. The expansion ratio was set by finely regulated com-

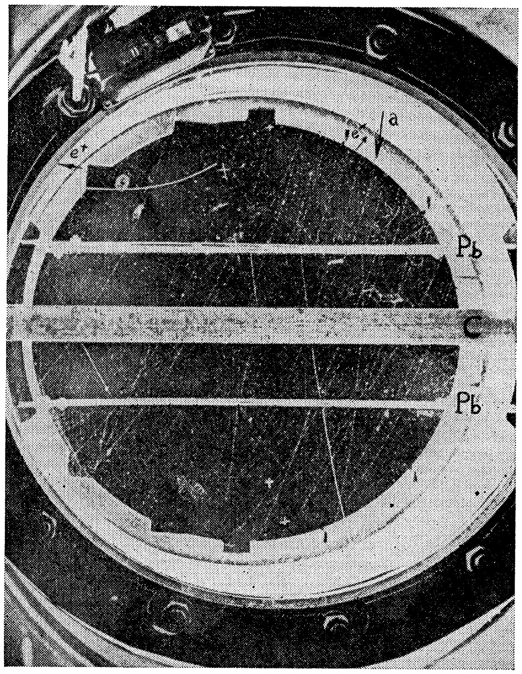

FIG. 1. The arrow (a) indicates incident meson which stops in carbon plate. A pair, marked e^+ and e^-, is observed in the backward direction. The pair axis intersects the projected meson trajectory within the carbon plate. A number of other events are marked on the picture.

---

[7] Anderson, Fermi, Martin, and Nagle, Phys. Rev. **91**, 155 (1953).

[8] R. Wilson and J. P. Perry, Phys. Rev. **84**, 163 (1951).

[9] W. O. Lock and G. Yekutieli, Phil. Mag. **43**, 231 (1952).

[10] M. Schein, *1953 Rochester Conference* (Interscience Publishers, New York, 1953).

[11] Fowler, Fowler, Shutt, Thorndike, and Whittemore, Phys. Rev. **91**, 135 (1953).

[12] A. Roberts and J. Tinlot, Phys. Rev. **90**, 951 (1953).

[13] Byfield, Kessler, and Lederman, Phys. Rev. **86**, 17 (1952).

[14] E. R. Gaerttner and M. L. Yeater, Rev. Sci. Instr. **20**, 588 (1949).

pressed air, fed to the underside of the rubber diaphragm through a null balance type regulator.[15]

C. Magnet

The magnet employed in this experiment is shown in Fig. 2. Helmholtz coils, 21-in. inside diameter, separated from each other by 6 in., were clad in a 2 in. thick mild steel casing around their periphery. The cloud chamber was mounted directly on the magnet. The coils were wound with copper conductor of rectangular cross section. A central hole in the conductor permitted efficient use of the circulating coolant. The magnetic field obtainable with an air-core magnet of this design is more than 30 percent higher than the field from standard Helmholtz coils of equivalent dimensions. Concurrently, no appreciable loss in field homogeneity is experienced.

The field generated in the useful region of the cloud chamber (a cylindrical volume 4 in. high and 14 in. in diameter), varied by less than 1 percent, peak to peak, from its mean value of $\sim$9000 gauss. To obtain this field value, a current of 1100 amperes, supplied by a 300-kw motor-generator set, was used. The time necessary to reach peak field values was 10 seconds.

A Leeds and Northrup "Speedomax" potentiometer provided a record of current passing through the magnet at the time of each cloud chamber expansion with an accuracy of 0.3 percent. A marker pip, incorporated in the instrument, indicated the exact time of expansion on the current (field) graph.

Absolute and relative field magnitudes were measured with a search coil and a General Electric integrating flux meter, both of which have been calibrated in a standard 5000-gauss field at the Columbia Radiation Laboratory.

D. Optics

Events were recorded with two cameras mounted on a light-tight cylinder placed on top of the magnet (Fig. 2). The Goertz Dagor 60-mm lenses were $51\frac{1}{4}$ in. above the mid-plane of the chamber. The use of this long object-lens distance eliminates, in most cases, the need for second-order corrections to curvatures and scattering angles. This may be easily verified from the reprojection formulas derived in Appendix C. The axes were 10 in. apart, and vertical. The film planes were horizontal, the film being offset slightly from the lens axes, in order to capture the whole image of the chamber. Pictures were recorded on Kodak Linagraph-Ortho, 35-mm film, with lenses set at $f/11$. Due care to prevent emulsion distortion and to bring out maximum contrast was taken during film development.

The reprojection system consisted of two commercial projectors, fitted with lenses similar to those in the cameras. Images were viewed on a large rear-projection screen (Recordak). The projectors were adjusted for unity magnification in the median plane.

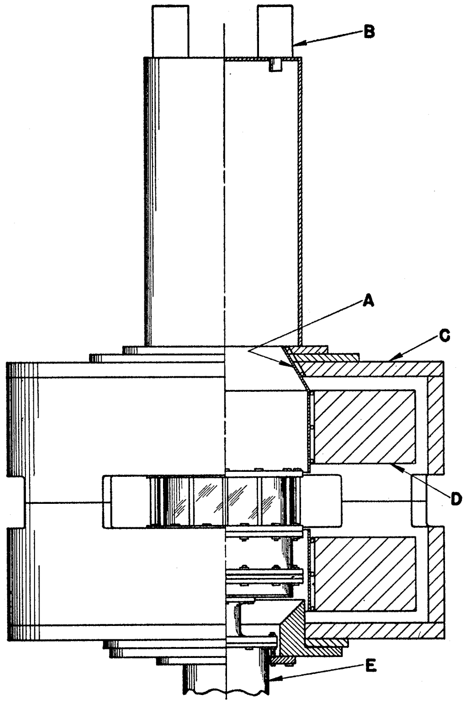

FIG. 2. Cutaway view of cloud chamber position in deflection magnet. A. Upper pole surface, B. camera, C. steel casing, D. coils, E. cloud chamber expansion mechanism. The drawing is approximately to scale. The outside diameter of the cloud chamber is 18 in.

The film carriage of one projector was mounted on a rotating-translating microscope stage. It was thus possible to bring the two stereoscopic images into register. The applications of this system to the various kinds of measurements is treated below, and in the Appendix.

III. ANALYSIS OF DATA

A. Criteria

Preliminary examination of the film indicated that the scanning of multiplate cloud chamber photographs, with an average of 12 tracks per picture, presents certain problems. In the present case, it was desired to obtain data yielding absolute reaction probabilities. In addition, it was hoped that clear evidence as to the existence, or nonexistence, of an unestablished reaction type would be found. The following scanning and accounting rules were therefore applied to insure impartial evaluation of the data.

(*1*) *Flux Counting Method*

(a) Pictures were scanned and flux counts made by at least two experienced observers, working independently. Final tallies varied by no more than 1 percent.

---

[15] Obtained from Moore Products, Philadelphia, Pennsylvania.

(b) All pictures containing more than twenty flux tracks were rejected, to permit clarity of observation.

(c) Only tracks making an angle δ with the normal to the first lead plate were accepted as flux, where $10°\leq\delta\leq 20°$, and 15° is the experimentally determined average angle of incidence (Fig. 1).

(d) Only tracks striking the first lead scattering plate between certain fiduciary marks were included in the flux count. These marks are sufficiently far removed from the cloud chamber rim (1.5 in. and 2 in.) that tracks passing undeflected through the scattering plate system could easily be followed all the way through, and that scattered tracks remained in the chamber for a sufficient distance to be clearly observed. The attenuation of the beam from plate to plate was determined from a sample count of 1000 tracks.

(e) The curvature of all apparent flux tracks was checked by template. Tracks were counted only if the particle momentum fell within the acceptable interval. To establish this interval, a momentum spectrum of tracks entering the cloud chamber was made. Tracks arriving outside the interval determined by the width of the histogram peak presumably had suffered energy loss in the materials surrounding the cloud chamber, or in the collimating slit.

(f) Tracks entering in fringe regions of the illumination were rejected, as only a small vertical deflection in a plate might have caused an apparent stopping. The height of the uniformly well illuminated region is 8 cm. At the boundaries the light intensity gradually decreases to zero in a space of $\sim$1.5 cm. Tracks entering in this fringe region therefore may be distinguished from more centrally located ones by their apparent faintness.

All tracks appearing faint relative to the main beam, in the opinion of the observers, were rejected. This scanning operation was the most difficult to carry out objectively. The independent records of individual observers, however, showed flux count discrepancies, per picture, of not more than 10 percent. The over-all totals showed a discrepancy of less than 1 percent. In order to account for possible errors incurred, a 5 percent error was assumed for the total flux count.

(g) The decision whether or not a given track was a "flux" or "nonflux" track was reached before the picture in question was scanned for events. It is, therefore, believed that the ratio between events observed and the number of good "flux" tracks is not subject to systematic bias.

(2) *Search for, and Measurement of Events*

(a) All pictures were scanned for events independently by at least two, and sometimes three observers. Each picture was scanned at least three times. The first scanning was $\sim$80 percent efficient relative to the last; the second $\sim$95 percent.

(b) Measurements of track curvature and scattering angles, as well as ionization estimates, where necessary, were performed twice, and, in the case of disagreements, three times.

(c) $\pi\rightarrow\mu$ decays in the gas of the chamber were recorded. Flux estimates from the number of $\pi\rightarrow\mu$ events observed,[16] agreed well with the actual corrected flux count.

B. Search for Charge-Exchange Scatterings

The search for charge-exchange scattering in complex nuclei was one of the objectives of the present experiment. Operationally, the reaction is characterized by the simple disappearance of a beam track. The π^0 decay time is $\cong 10^{-15}$ second. A neutral pion therefore travels only a negligible distance away from its point of origin before it decays.

The π^0 meson can be detected solely by means of the two photons arising from its decay. These photons may produce pairs in suitably located converting material. If the resulting electrons do not scatter greatly, the center line of each pair corresponds very well with the line-of-flight of its initiating γ ray. When the extrapolated pair center line coincides in space with the disappearance of a meson in a plate, the two are assumed to be associated. The kinematics of π^0 production are determined only if both resulting photons materialize.

All pictures were scanned for γ-induced electron pairs, associable with a stopped beam track. In practice, no double pairs appeared, and therefore methods of dealing with one pair only are outlined below.

The scanning adhered to certain restrictive criteria. Electron pairs corresponding to gamma rays emitted in the forward direction (within 20°) with respect to the stopped pion were rejected from the data. In this way bremsstrahlung effects due to any electron contamination of the meson beam were eliminated. Only electron pairs in which each electron had an energy ≥ 10 Mev were counted. This reduced multiple scattering effects which would increase errors in the center line extrapolation. In addition, the possibility of confusion with nuclear excitation γ rays are reduced. Events where materialization took place in the scattering plate in which the photon was produced were admitted to the total cross-section calculation. Direct decay of π^0 mesons into an electron pair cannot here be ruled out. This effect, however, is expected to be small,[17] except where it competes with conversion of photons directly in the carbon plate.

C. Scattering

Energy resolution was limited by the relatively small unobstructed areas of the cloud chamber within which curvature measurements could be made. In order to be classified into the inelastically scattered category, a meson was required to lose at least 40 Mev. In the case of short scattered tracks, due to rapid out-scattering

---

[16] Lederman, Booth, Byfield, and Kessler, Phys. Rev. **83**, 685 (1951).

[17] Lindenfeld, Sachs, and Steinberger, Phys. Rev. **89**, 531 (1953).

from the illuminated region, a definite change in track droplet density (at least by a factor of two) was required.

Track density determinations were based on a comparison of the track in question, with nearby tracks of beam energy.

Due to the finite angular spread of the incident beam, and the thickness of the scattering plates, it was very difficult to take systematic account of scatterings having projected angles <15° in both camera views. Accordingly, no attempts were made to locate these.

The radius of curvature of tracks was measured by fitting thin plastic templates, upon which suitable radii had been inscribed, with the projected track image. Projected angles of the curved tracks were measured by fitting templates to the initial and final track projections, and measuring the angular separation of the arcs with a 360° protractor. Average error of this measurement was ±1.0°.

Projected angle and dip angle measurements were made on all scatterings (Appendix).

The depth of any point on a track below a fiduciary plane was found by bringing the images of suitable marks, inscribed previously on the top glass, into exact register, and measuring the displacement of the two images of the droplet in question. This displacement is proportional to the height of the point (droplet) below the reference plane. Inclination of a given track was measured by this method. The vertical displacement between the two droplets on the track, and the (non-orthogonal) projected distance between them, together give the dip angle of their joining chord. The derivation of relevant formulas may be found in Appendix C. All measurements of momenta on inelastically scattered and incident particles are corrected for ionization loss in traversing the scattering plate. In the case of wide angle (near 90°) scattering, this correction attains considerable importance. It was not necessary to observe the 15° cut-off criterion in the case of inelastic scatterings. The characteristic changes in curvature and ionization observed in such events are adequate for their location.

D. Stars and Stops

Stars are easily located owing to the positive curvature and generally heavy ionization of the prongs. Proton energies are usually not measurable on account of the relatively short unobstructed path length available.

Apparent "stoppings" are due to a number of effects. A phenomenological classification may be made as follows:

(a) True stoppings, due to charge-exchange scatterings, or stars in which neutrons and/or photons only are emitted.

(b) Inelastic scatterings or stars in which the emitted particle has not enough energy to escape from the scattering plate.

TABLE I. Cross sections of observed reactions.[a]

	$\pi(1.40A^{\frac{1}{3}}\times10^{-13})^2$	Elastic $\theta>20°$	Inelastic $\Delta E>40$	Charge[b] exchange	Stars and stops	Total reaction
Carbon	325	179±18	70± 11	20^{+20}_{-10}	220± 40	308±43
Lead	2150	700±84	530±130	100^{+80}_{-40}	1840±350	2477±385

[a] All cross sections in millibarns.

[b] Cross sections calculated under assumption of isotropic photon distribution.

(c) Scatterings or stars in which the final particle leaves the illuminated depth before emerging from the plate.

(d) Tracks which arrive in fringe regions of the illumination, and pass out of it while in the scattering plate.

(e) Beam-contamination electrons radiating a high-energy, nonconverting photon.

It was desirable to obtain a good estimate of the number of stoppings falling into categories (a) and (b), as these constitute a significant fraction of the total number of nuclear absorption events. The inclination and relative height in the cloud chamber of all tracks appearing to stop were measured. In order to minimize contributions from (c) and (d), only stoppings occurring within a central, 3.5 cm high, fraction of the illumination were accepted into categories (a) and (b). The number of stoppings seen in this region was normalized to correspond to the total flux count.

It is not possible to determine directly the relative magnitude of the contribution from (c). The efficiency for loss from observation of elastically scattered particles has, however, been calculated as a function of scattering angle, for the whole illuminated height. This correction was applied to the total and differential elastic cross sections (Appendix).

Stops falling into category (e) were eliminated before the other corrections were applied. The number of these events was determined from the percentage of electron contamination in the beam. About 5 percent of the total intensity is due to electrons. This figure has been estimated from the number of particle-induced showers, of three or more final particles, observed in the lead

TABLE II. Compilation of charge exchange events.

Scattering material	Frame No.	Angle of emission of photon	Energy of photon in Mev
Carbon	20 448 C[a]	135°	35
	20 441 C	180°	70
	20 418 Pb	153°	65
	21 426 Pb	154°	49
Lead	20 816 Pb	72°	95
	21 139 Pb	115°	150
	20 033 C	155°	80
	20 593 C	122°	135
	21 039 Pb	24° (Event ambiguous, not counted)	

[a] The letter following the frame number indicates the converter plate.

plates.[18] In lead (0.6 radiation lengths), 2_{-1}^{+2} percent of the electrons stop without further trace. The number of electrons stopping in carbon is about one-tenth of this.

IV. EXPERIMENTAL RESULTS

The experimental results are summarized in Tables I and II, and in Figs. 3–7.

A total of 1500 pictures was used to obtain these data. (One example of inelastic scattering is shown in Fig. 8.) The flux count after beam corrections corresponds to 19 900 g/cm^2 of carbon traversal, and 33 100 g/cm^2 of lead. Three-hundred-and-three events were observed in lead; 451 events make up the total carbon statistics. The further distribution of categories within these statistics is contained in Tables I and II.

To obtain the total and differential elastic cross sections, correction factors, due to the observational efficiencies, were applied. The derivation of these factors may be found in the Appendix. The total inelastic cross section is, of necessity, only a lower limit, as discussed elsewhere.

All errors, as indicated on the curves or in the table, have been calculated by taking into account uncertainties in the counting statistics $[(N+1)^{\frac{1}{2}}/N\times 100$ percent], in the flux count and beam composition (5 percent), and in the applied corrections (variable). The rms sum of standard deviations has been used throughout this experiment.

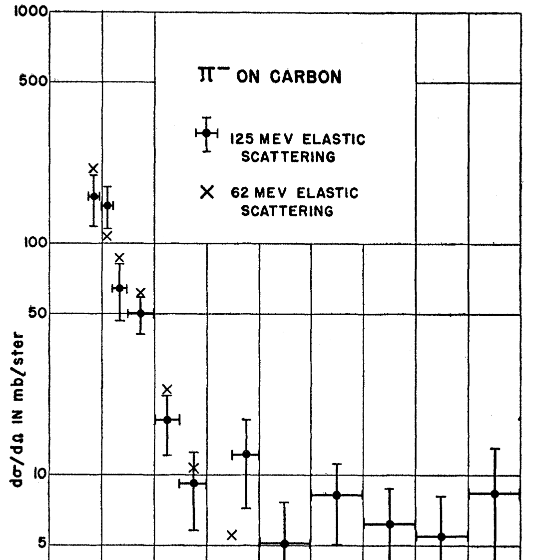

FIG. 3. Angular distribution of 125-Mev π^- elastic scattering in carbon. The crosses are points indicating the distribution for 62-Mev π mesons, and are included for comparison.

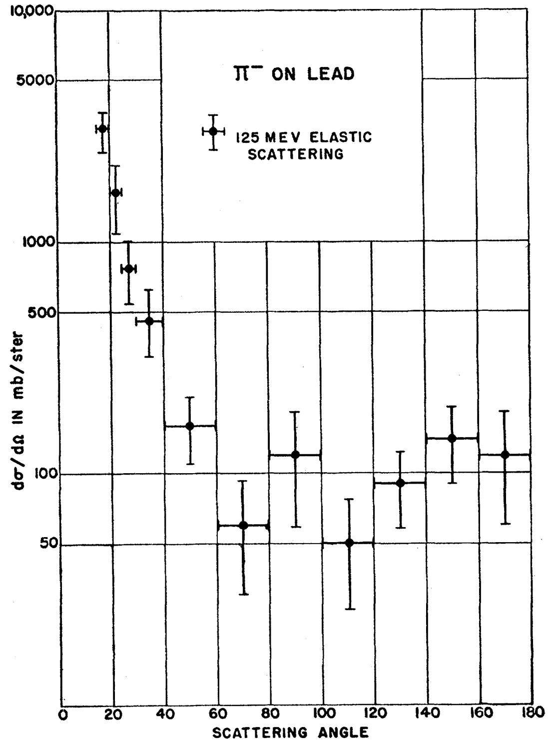

FIG. 4. Angular distribution of 125-Mev π^- elastic scattering in lead.

The correlated photon events observed are indicated in Table II. Because of the few events actually observed, and because of the statistical uncertainty in the conversion efficiency (Monte Carlo calculation—see Appendix), a very large experimental error must be quoted. The true number of charge-exchange events to be inferred from the observed number has been obtained with the aid of the Bernouilli probability distribution. If N is the true number of events, giving rise to n observed events, the a priori observation probability being p, then

$$n=Np\pm[N(1-p)p]^{\frac{1}{2}}.$$

One may solve for the desired number, N, to obtain, for $p\ll 1$,

$$N=\frac{1}{p}(n+\tfrac{1}{2})\pm\frac{1}{p}(n+\tfrac{1}{4})^{\frac{1}{2}}.$$

To obtain the total number of inferred charge-exchange events, it is necessary to sum-over all production mechanisms. In the sum, the N derived for each particular mechanism is weighted as the inverse square of its mean deviation, as given in the above equation. The carbon and lead events are of course treated separately.

---

[18] Results of Monte Carlo shower calculations for 200 Mev incident electrons were used. We are grateful to R. R. Wilson for the kind permission to utilize his shower graphs. See R. R. Wilson, Phys. Rev. 86, 261 (1952).

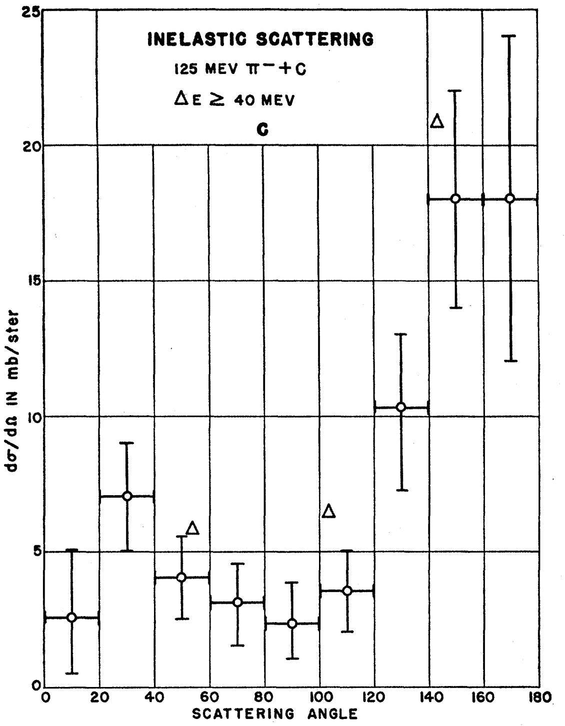

FIG. 5. Angular distribution for inelastic scattering in carbon. The triangles are comparison points describing the distribution of $\pi^{+}+p\rightarrow\pi^{+}+p$.

The total error is taken as the sum of the inverse squares of the partial errors, to the $-\frac{1}{2}$ power.

As the statistical probability for seeing the two direct carbon conversions is very small, in the light of the other events observed, direct "internal conversion" of the photons[17] arises as a distinct possibility in the present case.

V. DISCUSSION OF RESULTS

A. Elastic Scattering and Absorption

The "optical model," first discussed in these applications by Fernbach, Serber, and Taylor,[19] has been applied to the interpretation of high-energy neutron-[20] and pion-nucleus scattering.[13,21] The model, in its simplest form, treats the nucleus as a spherical region of uniform density, having a refractive index and absorption coefficient for the incident wave packet. The effect of the refractive index may be found[19] by considering the amplitude attenuation and change in phase of the incident wave, a procedure which neglects reflection effects. A rigorous solution of the wave equation in space, with appropriate matching to the region of complex potential, may also be made.[13] In this latter case, the approximations are inherent solely in the initial assumptions.[22]

Three parameters of the model, the radius, the real, and the imaginary part of the potential well may be used to fit the experimentally observed cross sections. The ultimate hope is that a good theory of the nucleus will naturally lead to a derivation of a model such as this, the parameters depending on the detailed properties of the nuclear constituents, and of their structure within the nuclear complex. At high bombarding energies, where binding effects presumably play minor roles, interpretation of the optical parameters in terms of elementary interaction processes, nuclear momentum distributions, and correlation effects is expected to be possible.[22] It is hoped, therefore, that interpretation of the present series of experiments in the light of the optical model may, apart from immediate conclusions, be of considerable use in the future.

Analysis of previous data[13] has yielded, for 60-Mev pions in carbon, optical parameters corresponding to a mean free path for absorption of the meson wave in nuclear matter of 8×10^{-13} cm, and a real potential well which is attractive and 20 Mev deep. The variation of these parameters with energy has been determined in the present experiment. It is found by an exact solution of the Schrödinger equation that a good fit may not be obtained here with the same parameters as in the 60-Mev case. Both the calculated angular distribution and

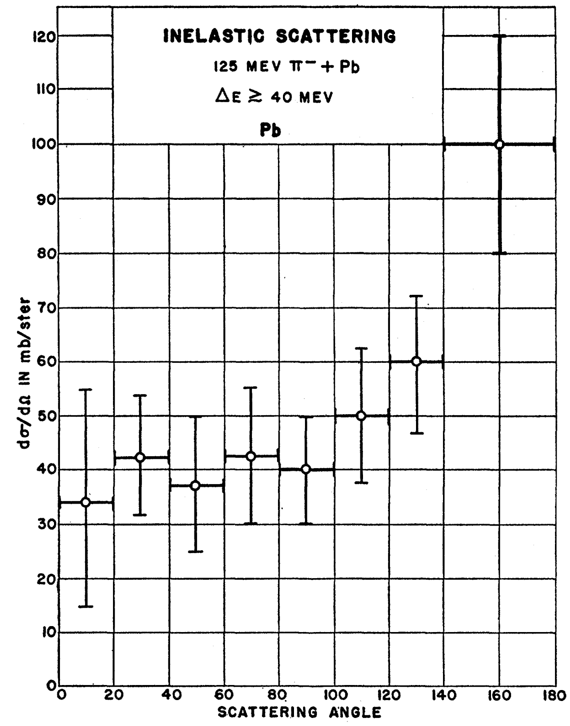

FIG. 6. Angular distribution of inelastic scattering in lead.

---

[19] Fernbach, Serber, and Taylor, Phys. Rev. **75**, 1352 (1949).

[20] J. DeJuren and N. Knable, Phys. Rev. **77**, 606 (1950).

[21] H. A. Bethe and R. R. Wilson, Phys. Rev. **83**, 690 (1951).

[22] K. M. Watson, Phys. Rev. **89**, 525 (1953). Also see N. C. Francis and K. M. Watson, Phys. Rev. **93**, 313 (1954).

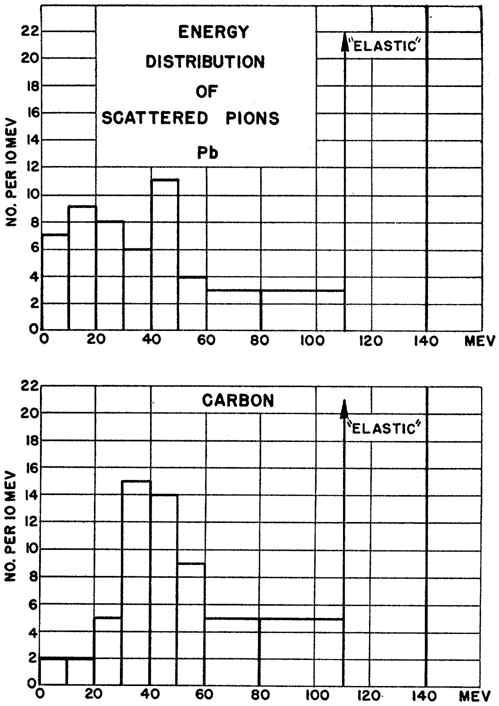

FIG. 7. Distribution of final energies of inelastically scattered mesons in lead and carbon. The data extend from 0 to ~85 Mev.

the total absorption cross section are found to differ from the observed magnitudes. A comparison of observed and calculated cross sections for carbon, together with the nuclear parameters used, is given in Table III. Since kR in this experiment is 3.9, the terms for which $L \geq 5$ do not contribute significantly to the cross sections. The method for calculating phase shifts is described in Appendix A. Since this is a charged-particle reaction, Coulomb wave functions should properly have been used. In carbon, however, the Coulomb parameter $\alpha = Ze^2/(\hbar\beta c) = Z/137\beta \simeq 0.05$ is small and hence affects the total wave function only very slightly. The statistical errors in the data for $\theta \geq 20°$ should therefore mask the Coulomb effect. In lead, $\alpha \cong 0.7$, indicating that correct calculations for this case must use the true Coulomb wave functions. Detailed calculations of this type are under way in this laboratory.[23]

TABLE III. Predictions of optical model for scattering of 125 Mev π^- mesons in carbon,[a] for a complex square well potential.

Curve number	Potential well[b] (assumed), Mev	Mean free path in nuclear matter[b] (assumed), cm	Total reaction σ(mb)[c] (calculated)
(1)	-36.6	4×10^{-13}	292
(2)	-30	3×10^{-13}	310
(3)	$+32$	3×10^{-13}	225
(4)	-21	9×10^{-13}	161
			observed experimentally: 308±43

[a] In these calculations, a nuclear radius of $1.4A^{\frac{1}{3}}\times10^{-13}$ cm has been assumed.

[b] A potential $V = \varphi - i\sigma$ Mev has been postulated. φ is the "potential well." This complex scattering potential leads to a complex propagation constant $k' = k + \frac{1}{2}iK$ within the nucleus. The "mean free path" is given by $(1/K)$.

[c] The angular distribution fits are best for curve (2).

In the selection of best fit parameter, the reaction cross section and angular distribution below 70° are given most weight. It is in this region that the model is expected to have more validity. Also, the presence of incoherent contributions may more seriously distort the diffraction pattern at large angles, where the differential cross section is small. We find carbon, at 125 Mev, to be represented by a real potential well, attractive and 30 Mev deep, and an imaginary well corresponding to a mean free path of 3×10^{-13} cm. Figure 3 and Table I give the data used here. The resulting parameters are consistent with the experimental results for lead. However, this is not a sensitive test of the model since the large size of the lead nucleus would lead to essentially geometric cross section for a large range of parameters.

The classical theory of the index of refraction relates the optical model parameters to the scattering properties of the constituent particles:

$$k'^2 = k^2 + 4\pi\rho f(0), \tag{1}$$

where $f(0)$ is the complex forward scattering amplitude in the elementary process and ρ is the density of scatterers. The availability of phase shifts as a function of energy in elementary pion-nucleon scattering[7,24] permits an examination of the relation of the optical parameters to the free scattering properties via the above equation. Table IV gives the result of computing $f(0)$ from the phase shift data at 80 and 155 Mev. Clearly, Eq. (1) does not allow for true absorption of the meson. The corresponding elementary process occurs in deuterium and has been observed as a function of energy.[25] Using the observed energy dependence of absorption in deuterium ($\sim p^2/v$) and the model for absorption in complex nuclei proposed by Brueckner, Serber, and Watson,[26] an estimate may be made for the mean free path for true absorption at 62 and 125 Mev. We get λ_a (62 Mev) $= 8\times10^{-13}$ cm and λ_a (125 Mev) $= 4.5\times10^{-13}$ cm. These values are similar in meaning to the quantities of Eq. (1) and may be added to the imaginary part in the form $R/2\lambda_a$. This has been done to obtain the calculated values given in Table IV.

It is characteristic of this model that the experimental mean free paths are much longer than those given by Eq. (1), whereas the real parts are in rough agreement. Recently, Watson[22] has examined the optical model quite generally. He finds that binding effects modify the scattering amplitude $f(0)$. These serve to reduce the imaginary part considerably. Any departure of ρ from a uniform distribution, as is possibly suggested by recent

---

[23] Pevsner, Williams, and Rainwater (private communication).

[24] Bodansky, Sachs, and Steinberger, Phys. Rev. **93**, 1367 (1954).

[25] Durbin, Loar, and Steinberger, Phys. Rev. **84**, 581 (1951).

[26] Brueckner, Serber, and Watson, Phys. Rev. **84**, 258 (1951).

experiments,[27] would also have a sensitive effect upon the nuclear mean free path.

The one difficulty which arises in the interpretation of the experimental data by means of the optical model is the poor fit obtained with the angular distribution beyond 70°. It has already been pointed out that the experimental points in the backward direction may be contaminated by slightly inelastic scatterings. Recent counter experiments,[23] with better energy resolution, still result in backward scattering considerably greater than that given by the model. The explanation of this effect may also be found in the strong angular dependence of the elementary nucleon scattering cross section. Although the elementary angular distribution is not expected to modify the optical model picture in a fundamental way, it may behave as a modulating form factor on the diffraction pattern. A Born approximation calculation of the scattering to be expected from a collection of nucleons has been performed, using the method described by Peaslee.[28] The result shows the expected rise in the backward direction, a reflection of the very strong backward scattering maxima observed in the elementary interaction. This data emphasizes the need for refinements in the theory of the optical model which will allow the inclusion of anisotropic elementary processes.

B. Inelastic Scattering

The energy and angular distributions of inelastically scattered mesons, presented in Figs. 5–7, appear as confirmation of earlier experiments by Bernardini *et al.*[1,2] which indicated two characteristic features of this process: strong angular dependence and large energy losses. An apparent peaking of the energy distributions of scattered mesons in carbon around 40 Mev is observed. However, the nature of the experimental arrangement is such as to favor just such distributions. The thickness of the scattering plates will certainly discriminate against the observation of very low-energy scattered mesons; the poor resolution at high energies tends to put particles suffering small energy loss into the "elastic" category. The experiment, therefore, is not to be taken as unambiguous confirmation of this effect.

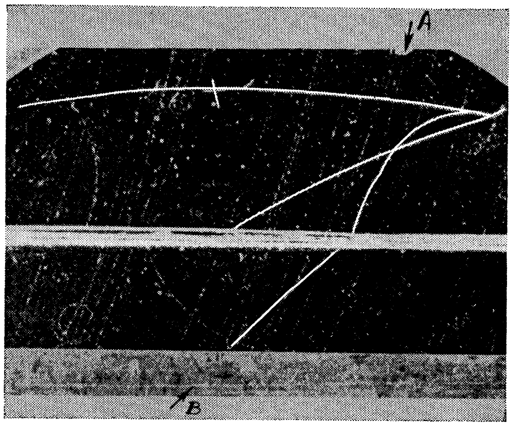

FIG. 8. Example of inelastic scattering in Pb. The incident meson A (130 ± 15 Mev) produces a single proton B and scatters through $\sim180°$ with an outgoing energy of <5 Mev. It stops in the gas, producing a sigma star of 2 protons and a recoil.

Our experiment suggests that the "quasi-elastic scattering" model[29] may yield a qualitative explanation of features observed in the angular distributions. In this model, the scattering process is assumed to result from interaction solely between the incident meson and a single bound nucleon. The applicability of the model is not obvious in the present case, since the meson wavelength is 0.86×10^{-13} cm, or $\sim\frac{1}{4}$ of the nuclear radius. A many-body interaction, resulting in scattered mesons, is not to be ruled out from a priori considerations. The strong nucleon correlation inside the nucleus, found necessary to account for meson absorption, places particular emphasis on this possibility.

The angular distribution of mesons inelastically scattered in carbon (Fig. 3), when compared to the angular distribution for the process $\pi^++p\rightarrow\pi^++p$,[7] nevertheless strongly suggests the use of the single-scattering picture. Additional evidence favoring this hypothesis is the energy dependence of the interaction. At 40 Mev, no inelastic scatterings have been observed.[2] At 60 Mev, $\sigma_{\text{inel}}\geq40$ mb,[13] and at 125 Mev, $\sigma_{\text{inel}}\geq72$ mb.

The data are insufficient statistically to establish a correlation between angle of scattering and energy loss. The pronounced preference for very large angle scattering in the elementary interaction would result in a reduced mean energy for the scattered particles. In a more detailed model internal nucleon motion or potential well effects could possibly decrease further the mean scattered energy.

The angular distribution in lead (Fig. 6) is smoother than that in carbon, an indication that in this larger nucleus multiple scattering effects are beginning to play a significant part. It is to be noted here also that the angular distribution statistics are somewhat biased experimentally against angles in the interval from 60° to 120°, and that hence some artificial depression of the differential cross section may occur in that region.[30]

TABLE IV. Calculated and observed nuclear parameters.

E (Mev)	V_{obs} (Mev)	V_{calc} (Mev)	λ_{obs} (Mev)	λ_{calc} (Mev)
62	20	28	8×10^{-13}	3×10^{-13}
125	30	30	3×10^{-13}	1.2×10^{-13}

---

[27] V. L. Fitch and J. Rainwater, Phys. Rev. **92**, 789 (1953); Hofstadter, Fechter, and McIntyre, Phys. Rev. **91**, 439 (1953).

[28] D. C. Peaslee, Phys. Rev. **87**, 862 (1952).

[29] R. Serber, Phys. Rev. **72**, 1114 (1947); P. A. Wolff, Phys. Rev. **87**, 434 (1952).

[30] The angular distribution of inelastically scattered high-energy negative pions in nuclear emulsions, where no discrimination against this angular region occurs, agrees well with the results of the present paper. S. Goldhaber and G. Goldhaber (private communication).

C. Charge-Exchange Scattering

High-energy photons, arising from the interaction of energetic pions with nuclei have heretofore[31] not been observed. It is not possible, with the data at hand, unambiguously to specify the production mechanism for these photons. Experience with the elementary pion-nucleon interaction, however, indicates that charge-exchange scattering, $\pi^-+p\rightarrow n+(\pi^0\rightarrow 2\gamma)$, is the most probable mechanism. This view is strengthened by a detailed balancing calculation which shows that the cross section for the only possible competing process $\pi^-+p\rightarrow n+\gamma$ has, in the case of the nucleon interaction, a magnitude of only 2 percent that of the charge-exchange cross section.[7] Discounting, then, the possibility that these photons arise through other mechanisms, one may consider the charge-exchange reaction to have been established under the conditions obtaining in this experiment.

The magnitude of the observed effect, although considerably smaller than that for the comparable case of inelastic scattering, may be understood in the light of a simple assumption. Under the hypothesis that, in the first approximation, the charge-exchange and inelastic scattering cross sections for the present high bombarding energies are affected by nuclear structure in entirely similar ways, one may obtain an estimate of their relative size through use of the known[7,24] elementary cross sections. The ratio, R, obtained for the present case, is

$$R=\frac{\sigma_{\text{ch.ex.}}A(z)}{\sigma_{\text{inel.}}A(z)}=\frac{Z\sigma(\pi^-+p\rightarrow\pi^0+n)}{Z\sigma(\pi^-+p\rightarrow\pi^-+p)+N\sigma(\pi^++p\rightarrow\pi^++p)},$$

where it has been assumed that $\sigma(\pi^++p\rightarrow\pi^++p)=\sigma(\pi^-+n\rightarrow\pi^-+n)$. The calculated R, then, is 0.3 for carbon and 0.2 for lead. The experimental ratios observed were $R_{\text{C}}\cong 0.26$, and $R_{\text{Pb}}\cong 0.20$.

Two qualitative points may be made as to the modification of R by binding effects. The interference between neutron and proton scattering for pions incident on deuterium has been calculated by Brueckner.[32] He finds destructive (Pauli) interference for charge exchange, constructive for ordinary scattering. To the extent that such a process takes place in carbon, it may serve to reduce the calculated R.

The Pauli principle, in addition, acts to suppress the forward part of the free scattering form factor, since forward scattering implies only small momentum transfer to the struck nucleon. The ratios of backward to forward scattering in elementary collisions have been observed by the Chicago group.[7] They find, at 135 Mev,

$$r(\pi^-\rightarrow\pi^0)=2.3,\quad r(\pi^-\rightarrow\pi^-)=1.0,\quad r(\pi^+\rightarrow\pi^+)=3.9.$$

The Pauli principle, therefore, acts in this case to suppress a larger fraction of the total charge exchange than of the inelastic scattering.

It is of interest to compare these results with other workers. Lock and Yekutieli[9] deduce a large charge-exchange cross section (~30 percent geometric) for high-energy mesons (<160 Mev) in nuclear emulsion. Since the elementary cross section increases with energy up to 220 Mev, this may still be consistent with our results. Shutt[12] and co-workers obtain a charge-exchange cross section of 60 mb for 105-Mev pions in helium. This would indicate a very strong effect due to nuclear structure. Tinlot and Roberts at 40 Mev, observe a very small π^0 yield from carbon, ~ few millibarns. Schein[10] has observed high-energy electron pairs emerging from π^--induced stars in nuclear emulsion. The observed frequency (1 per 500 stars) is consistent with our results (5 percent geometric or 10 percent of star production) and the fact that one out of 80 π^0's will decay into a photon and an electron pair.[17]

We would like to express our thanks to Mr. Hugh Byfield for his contributions in the planning and execution of this experiment, and in the construction of the apparatus. We wish to acknowledge many discussions with Professor Serber, Professor Rainwater, and Professor Steinberger, concerning the various aspects of this experiment. Mr. Kenneth Rogers assisted greatly in the scanning and calculations.

One of us (JOK) would like to express appreciation to the Radio Corporation of America's Laboratories, for their support in the final phases of the research. The main body of the research was supported by the joint program of the U. S. Office of Naval Research and the U. S. Atomic Energy Commission.

APPENDIX

A. Calculation of Complex Square Well Scattering Amplitudes

The significance of complex potentials has been given by Bethe.[33] If $V=\phi+i\sigma$, the continuity equation becomes

$$\frac{\partial}{\partial t}|\psi|^2-\nabla\cdot\mathbf{S}-2\frac{|\psi|^2}{\hbar}\sigma=0,$$

where ψ is the wave function, and $\mathbf{S}$ is the usual probability current density. A potential representing attraction and absorption may, therefore, be represented by

$$V=-|\phi|-i|\sigma|.$$

Assuming that V transforms with the total energy, E, the relativistic equation determining the meson wave

---

[31] Recent results of Tinlot, Roberts, and Spry (private communication), indicate a cross section for charge exchange of 3–5 mb for 40-Mev negative pions, incident on Li, Be, and C.

[32] K. A. Brueckner (to be published).

[33] H. A. Bethe, Phys. Rev. **57**, 1125 (1940).

propagation vector $\mathbf{k}'$, in the field of a nucleus is

$$c^2\hbar^2k'^2=E^2+V^2-m^2c^4-2EV.$$

If $E\gg V$,

$$c^2\hbar^2k'^2\cong c^2\hbar^2k_0^2-2EV,$$

where

$$k_0^2=(E^2-m^2c^4)/c^2\hbar^2.$$

With these assumptions one obtains

$$k'=\left[\left(k_0^2+\frac{2E\phi}{\hbar^2c^2}\right)^2+\left(\frac{2\sigma E}{\hbar^2c^2}\right)^2\right]^{\frac{1}{4}} \cdot\exp\left[\frac{i}{2}\tan^{-1}\left(\frac{2\sigma E}{\hbar^2c^2k_0^2+2\phi E}\right)\right].$$

One may then write a quasi-relativistic Schrödinger equation

$$\nabla^2\psi+k^2\psi=0,$$

where $k=k'$, $r<R$, and $k=k_0$, $r>R$, R being the radius of the potential well.

The scattering amplitude for a partial wave solution of the Schrödinger equation is

$$f(\theta)=\frac{1}{2ik_0}\sum_l(2l+1)[\eta_l-1]P_l(\cos\theta),$$

where η_l is determined from matching the inside and outside radial wave functions at the nuclear boundary. The radial wave may be written[34]

$$B_l^{(0)}(r)=A_l[\cos\delta_l j_l(k_0r)-\sin\delta_l n_l(k_0r)],\quad r\geqslant R,$$
$$B_l^{(i)}(r)=C_l[j_l(k'r)],\quad r\leqslant R.$$

Defining $\eta_l=\exp(2i\delta_l)$, one may rewrite the first equation,

$$B_l^{(0)}(r)=D_l[h_l^{(2)}(k_0r)+\eta_l h_l^{(1)}(k_0r)],$$

where j_l, n_l, and $h_l^{(1),(2)}=j_l\pm in_l$, are spherical Bessel functions. Equating the logarithmic derivatives of $B^{(i)}$ and $B^{(0)}$ at R, and solving for η_l, one obtains

$$\eta_l=\frac{k_0[h_l^{(2)}(k_0R)]'j_l(k'R)-k'h_l^{(2)}(k_0R)[j_l(k'R)]'}{k'h_l^{(1)}(k_0R)[j_l(k'R)]'-k_0[h_l^{(1)}(k_0R)]'j_l(k'R)}.$$

Primed brackets denote differentiation with respect to the argument of the Bessel function. As k' is complex, calculation by means of this formula is quite involved. Considerable simplification is achieved through use of a recursion relation for complex half-order Bessel functions which has been given by Aden.[35] It may be shown that if one defines $\sigma_l(x)\equiv d/dx\log[xj_l(x)]$, that

$$x\sigma_l(x)=\frac{x^2+l[x\sigma_{l-1}(x)]-l^2}{l-x\sigma_{l-1}(x)},$$

where $x=a+ib$ and

$$\sigma_0(x)=[\sin2a-i\sinh2b][\cosh2b-\cos2a]^{-1}.$$

The expression for η_l may now be modified to permit use of the recursion relation:

$$-\eta_l=\frac{k_0R[h_l^{(2)}(k_0R)]'+h_l^{(2)}(k_0R)[1-k'R\sigma_l(k'R)]}{k_0R[h_l^{(1)}(k_0R)]'+h_l^{(1)}(k_0R)[1-k'R\sigma_l(k'R)]}.$$

In the actual calculation, tables[36] dictating a final revision of the form of the equation were used. In this final form, the calculation of a set of five η's for a given meson energy and set of nuclear parameters became a relatively minor undertaking. This form was

$$-\eta_l=\frac{\tan\delta_l(\tan\alpha_l-z_l)-i(z_l-\tan\beta_l)}{\tan\delta_l(\tan\alpha_l-z_l)+i(z_l-\tan\beta_l)},$$

where

$$\tan\alpha_l(x)=-xj_l'(x)[j_l(x)]^{-1},$$
$$\tan\beta_l(x)=-x[\eta_l(x)]'[\eta_l(x)]^{-1},$$
$$\tan\delta_l(x)=-j_l(x)[\eta_l(x)]^{-1},$$
$$z_l(kR)=1-kR\sigma_l(kR),$$
$$x=k_0R.$$

The first three of these quantities are tabulated, and the last may easily be calculated by means of the recursion relation.

B. Efficiency for Photon Conversion

Photons arising in the carbon may materialize in the carbon plate itself, or in one of the two lead plates. Photons originating in one of the lead plates may convert in it, in the other lead plate, or in carbon. It is necessary to account for all these possibilities in the derivation of the photon observation efficiency.

The calculation of these probabilities combines the solid angle efficiency factor and the elementary conversion probability. In general, it involves numerical integration and/or the averaging of efficiencies over representative photon production and materialization points.

The element of solid angle, $d\omega$ subtended at the origin by an element of area, $dxdz$, at (x,z), in a plane $y=y_0$, is given by

$$d\omega=y_0\frac{dxdy}{(x^2+y_0^2+z^2)^{\frac{3}{2}}}.$$

Defining $\theta_i=\tan^{-1}(x_i/y_0)$, one may write the total solid angle included between θ_1, θ_2 and the heights z_1 and

---

[34] L. I. Schiff, *Quantum Mechanics* (McGraw-Hill Book Company, Inc., New York, 1949), Chap. V.

[35] A. L. Aden, J. Appl. Phys. **22**, 601 (1951). A more general recursion relation, from which the one used in this paper was derived, is given by L. Infeld, Quart. Appl. Math. **5**, 113 (1947).

[36] *Scattering and Radiation from Circular Cylinders and Spheres* (U. S. Navy Department of Research and Inventions, July, 1946).

z_2, in the plane $y=y_0$, as

$$\Omega(\theta_1,\theta_2)=\sum_{i=1}^{2}\sum_{j=1}^{2}(-1)^{i+j}\tan^{-1}\left[\frac{x_iz_j}{y_0}(y_0^2+x_i^2+z_j^2)^{-\frac{1}{2}}\right].$$

The conversion efficiency, for cases in which a photon emerges from one of the scattering plates and converts in another, was calculated in the following way: a point of origin for the photon was chosen. The plate of destination was divided into intervals (θ_1,θ_2), the average conversion efficiency for each interval being determined from the appropriate transition curve. The solid angle and conversion efficiencies were then multiplied for each interval, and the products summed over the whole conversion plate. The calculation was repeated over a number of representative points (twelve for carbon) in the plate in question, the mean of these efficiencies then giving the final result.

The efficiencies for conversion directly in the plate of origin of the photons similarly were calculated, taking into account the available height of the illuminated region, as well as the relative magnitudes of the solid angle and conversion path. All efficiencies have been calculated under the assumption of isotropic photon angular distribution.

The transition curves needed in this experiment must give the probability, as function of converter thickness, of ~100 Mev γ-ray materialization, each resulting pair member having an energy $\geqslant 10$ Mev. To minimize secondary effects, it is required that the electrons have charge of opposite sign.

Professor R. R. Wilson has very kindly permitted us to use the data from his Monte Carlo calculations to obtain the desired transition curve. The efficiency in lead, as derived from 142 individual shower graphs,[17] rises steeply from zero to ~30 percent in the interval from zero to 1 radiation length. A relatively slow fall-off occurs beyond this thickness, the efficiency at 2 radiation lengths being ~18 percent.

The conversion efficiency for carbon was calculated under the assumption that for the thickness in question pairs once produced do not reradiate. The average ionization energy loss of pair electrons was taken into account.

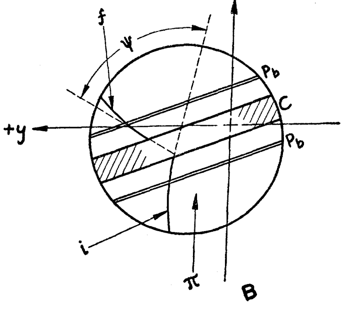

FIG. 9. Coordinate system for deriving projection formulas. $\pi\rightarrow$ indicates direction of incident beam, i—incident pion, f—scattered pion, ψ—projected scattering angle, Pb—lead plates, C—carbon plate.

If W_γ is the energy of the initial photons, ϵ the ionization loss of minimum ionizing electrons/cm of carbon, t the thickness at which the pair is produced, D the total thickness (in cm) of the carbon, λ_p the mean free path for pair production,[37] E the initial energy of the positron, and A a factor near unity, due to the pair production spectrum, then the efficiency is given by η, where

$$\eta=\frac{A}{W_\gamma}\int_0^D dt\frac{e^{-t/\lambda_p}}{\lambda_p}\int_{(D-t)\epsilon+10}^{W_\gamma-[(D-t)\epsilon+10]}dE.$$

In the region of carbon thickness of interest, and for $W_\gamma=100$ Mev, the result of the integration may be expressed by the simple formula $\eta=(1.1D+1.74)$ percent.

The per photon conversion efficiencies are:

Pb_1 or $\text{Pb}_2\rightarrow\text{C}$ 1 percent (each plate),

$$\left.\begin{matrix}\text{Pb}_1\rightarrow\text{Pb}_2\\ \text{or Pb}_1\rightarrow\text{Pb}_2\end{matrix}\right\}\text{3.4 percent (both plates together),}$$

$$\left.\begin{matrix}\text{Pb}_1\rightarrow\text{Pb}_1\\ \text{Pb}_2\rightarrow\text{Pb}_2\end{matrix}\right\}\text{12.9 percent (each plate),}$$

C→C 0.6 percent,

C→(Pb_1 or Pb_2) 7.6 percent (both plates).

The element to the left of the arrow indicates the plate of origin of the photon, the element to the right, the plate of conversion. Because of the method of calculation, and the 20 percent statistical uncertainty in the lead transition curve, a possible error of ~30 percent must be allowed for in these efficiencies.

C. Measurement of Space Angles

1. Stereo Height Determination

Any point T, within the cloud chamber, is projected onto the scanning screen from two film images, through two lenses, L and Λ. The film images of a top glass fiduciary mark F are projected similarly. It is desired to measure the distance s between the planes containing F and T, respectively. If the distance between the projections of F is δ_x, and that between the projections of T is δ_0, then the value of s is determined by $\Delta=\delta_x-\delta_0$. In practice δ_x is made to vanish by suitable translations and rotations of one film relative to the other. When this is done, one measurement suffices to determine s.

Consideration of the geometry easily shows that the stereo depth calibration equation is

$$s=\frac{p\Delta}{(2lf/p)-\Delta},$$

---

[37] λ_p for carbon has been obtained by extrapolating the data of J. L. Lawson, Phys. Rev. **75**, 433 (1949).

where $2l$ is the distance between lenses, p the distance between top glass and lens plane, and f the distance between scanning screen and lens plane.

2. *Projection Formulas*

It is necessary to account for the fact that pictures are not recorded from infinity. In many cases, depending on the location and type of the event in question, the nonorthogonality of the projection does not permit the use of standard orthogonal projection formulas. Accordingly, the relative location in the cloud chamber of all such events has been measured, and used to arrive at the correct scattering geometry.

The information needed to calculate correctly the space and dip angles of any scattered track consists of the projected angle relative to the incident track, a projected length on the scattered track, the relative heights in the cloud chamber of the ends of this length, and the position of this segment relative to the vertical projection of the recording lens onto the screen. Figure 9 shows the coordinate system used in the derivation of the formulas. The origin is located at the foot of the perpendicular from screen to lens; the x axis is chosen along the direction of the incident track, marked i. The final track, marked f, makes a projected angle ψ with the incident direction. The z direction is upward, out of the paper. Let: D_T = true length of scattered track segment, D_0 = projected length of scattered track segment, $(0,0,h)$ = projecting point (camera lens), ψ = projected scattering angle, Θ = true scattering angle, δ = true dip angle, (x_i, y_i, z_i) the space coordinates of the scattered track segment, and (x_i^0, y_i^0), $(i=1, 2)$ = the coordinated defining the projection onto the screen of the scattered track segment. Let $(x_1^h, y_1^h, z_1^h) = (0,0,h)$. Then the projection of the track onto the screen gives

$$x_1^0 = x_1 h/(h-z_1), \quad y_1^0 = y_1 h/(h-z_1)$$

$$x_1 - x_2 = x_1^0 - x_2^0 - (1/h)(z_1 x_1^0 - z_2 x_2^0)$$

$$\Delta x = \Delta x^0 (1 - z_2/h) - (x_1^0/h)\Delta z. \quad \text{(Similarly for } \Delta y.\text{)}$$

Then

$$\begin{aligned} D_T^2 &= (\Delta x)^2 + (\Delta y)^2 + (\Delta z)^2 \\ &= D_0^2 (1 - z_2/h)^2 + (\Delta z)^2 [1 + (x_1^{02} + y_1^{02})/h^2 \\ &\quad - 2(D_0 \Delta z/h)(1 - z_2/h)(x_1^0 \cos\psi + y_1^0 \sin\psi)], \end{aligned}$$

where $D_0^2 = (\Delta x^0)^2 + (\Delta y^0)^2$. Then $\delta = \sin^{-1}(\Delta z/D_T)$ and

$$\Theta = \cos^{-1}\left[\frac{D_0}{D_T}\cos\psi\left(1 - \frac{z_2}{h}\right) - \frac{x_1^0}{h}\cdot\frac{\Delta z}{D_T}\right].$$

Appropriate simplifications may be made depending on the magnitude of the parameters.

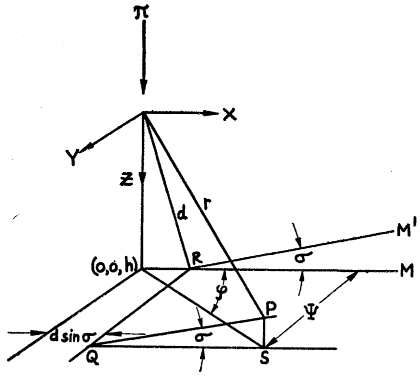

FIG. 10. Construction for calculation of number of scatterings missed due to the finite height of the illuminated region. The origin is situated at the scattering point of the incident meson. The z axis is directed along the initial horizontal flight direction, the y axis points vertically upward. The x axis is horizontal and perpendicular to both. Plane M', determined by PQR, represents the far boundary of the scattering plate. The scattering occurs at a distance d above it. Plane M is normal to the incident flight direction, and a distance $z=h$ below the scattering point. OP represents the scattered meson, and has polar angles θ, φ. P is the intersection of the rear bounding plane of the scattering plate and the scattered track.

D. Detection Efficiency for Elastic Scatterings

1. *Efficiency Calculation for 15° Projected Angle Cutoff*

During scanning, only scatterings with projected angles $\psi \geqslant 15°$ are recorded. This means that, in cases where the azimuth angle φ is near 0° or 180°, scatterings with space angles θ appreciably greater than 15° may be lost from observation.

To calculate the efficiency of observing an elastic scattering into θ, one must first obtain $\varphi = \varphi(\psi)_{\theta\ \text{const}}$. The efficiency of observation then becomes, in any given azimuthal quadrant,

$$E(\theta) = 1 - [\varphi_\theta(\psi = 15°) - \varphi_\theta(\psi = 0°)]\frac{2}{\pi}.$$

Let λ be the angle between the vertical direction and a ray drawn from the observing camera lens to a point determined by the intersection of the vertical plane containing both lenses, and the scattered track. It may easily be shown that, for cases where θ is less than $\sim 70°$ (at larger θ, other corrections predominate), one has

$$\varphi(\psi) = \sin^{-1}(\tan\psi \cot\theta \cos\lambda) + \delta.$$

Averaging over-all scattering positions in the cloud chamber, and over both camera positions, one finds that for the present geometry the effect of $\cos\lambda$ in the bracket is quite negligible. The over-all efficiency, to a very good approximation, is equal to that obtaining in the case of one projection point (camera) at an infinite height above the chamber. It is given by

$$E(\theta) = 1 - \frac{2}{\pi}\sin^{-1}(\tan 15° \cot\theta).$$

2. Efficiency Calculation for Scatterings Missed because of the Finite Height of the Illuminated Region

Tracks are incident on the scattering plate system at an angle $\sigma \simeq 15°$ with the normal. The height of the illuminated region is $\simeq 8$ cm. This situation is represented in Fig. 10. For the case illustrated, the coordinates of P are

$$\begin{aligned} x_p &= r\sin\theta\sin\varphi = d\sin\sigma + l\cos\sigma, \\ y_p &= r\sin\theta\sin\varphi, \\ z_p &= r\cos\theta = d\cos\sigma - l\sin\sigma, \ [\langle QP\rangle_{\mathrm{Av}} = l]. \end{aligned}$$

In the drawing, $y_p = Y$, which indicates that P is at the boundary of the illumination.

The efficiency for observing a scattering through an angle θ, taking place at a depth of d centimeters into the scattering plate, is

$$E(\theta) = \frac{1}{2\pi}[\varphi(Y,d)_+ + \varphi(Y,d)_- + \varphi(8-Y,\, d)_+ + \varphi(8-Y,\, d)_-],$$

where the subscripts refer to the two cases $\cos\varphi = \pm|\cos\varphi|$.

Solving the above coordinate equations, for the case $y_p = Y$, one obtains

$$\cos\varphi = \sin\varphi\left[\frac{\sin\sigma\tan\sigma + \cos\sigma}{\tan\sigma}\right]\frac{d}{Y} - \frac{\cot\theta}{\tan\sigma},$$

from which the explicit expression for $\varphi(Y,d)$ is easily derived. This is then inserted into $E(\theta)$. To obtain the desired efficiency, numerical averaging over representative (Y,d) is carried out.

As may be expected $E(\theta) \simeq 1$ for θ small. It is a minimum for $\theta = 75°$, and rises slowly for $75° < \theta \leqslant 90°$. In the latter case the track emerges through the front of the scattering plate. $E(\theta)$ is symmetric about $\theta = 90°$.

No correction need be applied to account for tracks passing out of the cloud chamber before emerging from the scattering plate (within the illuminated height). Owing to the track entrance criterion, and the small height of the illumination together with the narrowness of the scattering plate relative to the cloud-chamber width, the magnitude of this correction is negligible.

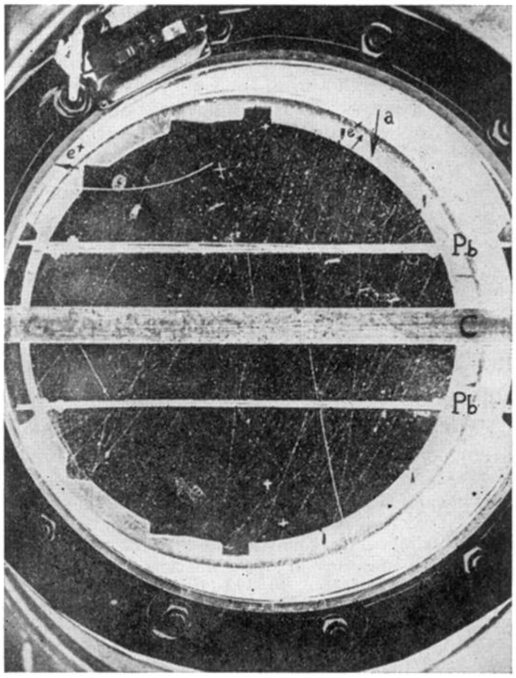

FIG. 1. The arrow (a) indicates incident meson which stops in carbon plate. A pair, marked e^+ and e^-, is observed in the backward direction. The pair axis intersects the projected meson trajectory within the carbon plate. A number of other events are marked on the picture.

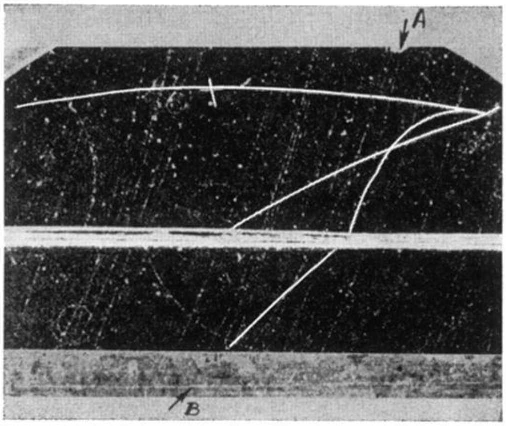

FIG. 8. Example of inelastic scattering in Pb. The incident meson *A* (130±15 Mev) produces a single proton *B* and scatters through ~180° with an outgoing energy of <5 Mev. It stops in the gas, producing a sigma star of 2 protons and a recoil.